



Synthesis, characterization, investigation of mesomorphic properties and DFT studies of a new 2,5-(dimethoxy)-2-[[4-(dodecyloxy)phenyl]imino]methyl]benzene): a material liquid crystal for optoelectronics

Hülya Elmalı Gülbaş¹ · Emine Tanış² · Ali Antepli³

Received: 15 April 2020 / Accepted: 31 July 2020 / Published online: 12 August 2020
© Springer Science+Business Media, LLC, part of Springer Nature 2020

Abstract

In this article, synthesis, characterization and mesomorphic properties of a new calamitic liquid crystal, 2,5-(dimethoxy)-2-[[4-(dodecyloxy)phenyl]imino]methyl]benzene) (DDPIMB) are described. The phase transition temperatures of the DDPIMB mesomorphic compound have been carried out by differential scanning calorimetry and optical polarizing microscopy. Geometry optimization calculations have been made for the two possible isomers as cis and trans of DDPIMB using the DFT/B3LYP/6-311++G(d,p) level of theory. According to the theoretical calculation results, trans isomerism was found more stable than cis isomerism. Therefore, all theoretical calculations were made for the trans-isomer and compared to the observed results. Vibrational assignments of the observed infrared spectra of title compound were carried out based on the calculated potential energy distributions (PEDs). The electronic properties of the DDPIMB were shown on the TD-DFT/B3LYP level. The optical behavior of the liquid crystal DDPIMB was determined through basic optical parameters, nonlinear optics (NLO) properties and dipole moments. Moreover, frontier molecular orbitals and molecular electrostatic potential (MEP) were determined to define the chemical activity of the headline molecule. The obtained results showed that this liquid crystal is a candidate material that can be used in NLO, optics and optoelectronic technology.

1 Introduction

The liquid crystal (LC) materials have been unique class of soft materials because of their physical properties, showing mobility of liquids and order of solid. Thermotropic liquid crystals have been a very widely studied topic because of their unique optical and electro-optical properties [1]. The first commercially significant thermotropic liquid crystals have been calamitic mesogens which have a rod-like molecular geometry. Calamitic mesogens are extraordinary materials for technological applications used in various fields such as chemistry, biology, electro-optics, optics, thermally conducting materials, and fast switching devices [2–5].

The design of a new calamitic mesogen for technological applications have emerged with suitable selection of core fragments, linking groups and terminal functional groups [6]. The different linking units such as azo, ether, ester and imine have been used in between aromatic rings. The imine linking groups have been widely used in thermotropic liquid crystals [7]. The LC properties of thermotropic calamitic mesogens have been widely affected by the nature of structure of terminal chains, such as being the alkyl, alkyloxy, perfluorinated chain or ester and the length of terminal chains [8]. Also in the literature, there are studies investigating the effect of imine-based calamitic liquid crystals on LC phases and involving the systematic study of three ring imines and salicylaldimine's, at least one of which is chiral or carrying two terminal alkoxy chains, both of which are not chiral [9–15]. The new imine liquid crystal molecule DDPIMB in this study is formed of two benzene ring cores comprising with imine linking units, n-dodecyloxy group in the one of the terminals and 2,5-dimethoxy groups as other side. The effect of position of the dimethoxy group and the length of dodecyloxy group for mesomorphic properties of this type of liquid crystal molecule have been investigated.

✉ Emine Tanış
eminetanis@ahievran.edu.tr

¹ Department of Chemical Technology, Banaz Vocational School, Usak University, Usak, Turkey

² Department of Electrical Electronics Engineering, Faculty of Engineering and Architecture Kırşehir Ahi Evran University, Kırşehir, Turkey

³ Usak University, Usak, Turkey

The packing of molecules in mesogens have taken place in a few ways leading to varied phases of different order and symmetry between the crystalline and isotropic phases. The rod-like molecules self-assembled into different liquid crystalline phases as a layered smectic phase (Sm) or non-layered nematic phase [16].

The differential scanning calorimetry (DSC), optical polarizing microscopy (PM) and X-ray diffraction (XRD) methods are commonly used experimental techniques for detecting the structural properties of liquid crystal phases [17].

There are many theoretical studies that shed light on the theoretical, optical, electronic, and structural properties of liquid crystals [18–24]. These theoretical approaches are also widely used to assign and interpret experimental infrared and Raman results [25, 26].

In this study, 2,5-(dimethoxy)-2-[[4-(dodecyloxy)phenyl]imino]methyl]benzene) (DDPIMB) was successfully synthesized, and a mesomorphic compound was characterized. The mesomorphic properties of DDPIMB were determined by optical polarizing microscopy and differential scanning calorimetry. With computational methods, vibrational wavenumbers, chemical shifts and UV–Visible spectroscopic analyses were performed and compared to existing experimental data. Additionally, electronic properties such as molecular orbital energies, energy gap, chemical reactivity identifiers such as chemical hardness, chemical potential, electronegativity and electrophilicity index, which are also non-linear optical properties, and MEP were calculated and discussed in detail. The fundamental optical parameters such as absorption band edge, optical band gap (E_g) and refractive index (n) of the DDPIMB were obtained by semi-empirical relations based on measured energy gap (E_g) data.

2 Experimental

The purity of the DDPIMB was determined by thin layer chromatography (TLC). The DDPIMB was characterized by using conventional spectroscopic methods. Ultraviolet–visible (UV–Vis) spectra were measured in quartz cell chloroform as the solvent using an Agilent 8453 spectroscope. Fourier transform infrared (FT-IR) measurements were taken in the range of 4000–400 cm^{-1} with ATR equipment using a Perkin-Elmer FT-IR spectroscopy. ^1H -NMR and ^{13}C -NMR measurements were made on a Bruker 400 MHz device in chloroform solvent with tetramethyl silane (TMS) as internal reference. The thermal transition properties were characterized by using differential scanning calorimetry (DSC) in a Perkin-Elmer DSC-7 device at heating and cooling rates of 10 $^\circ\text{C}/\text{min}$ up to 120 $^\circ\text{C}$. The texture of the imine mesogens were observed by using a Leitz Laborlux 12 Pol optical polarizing microscope (PM), equipment with

Linkam THMS 600 hot stage and Linkam TMS93 temperature controller.

2.1 Materials

p-Nitrophenol, 2-butanon, 1-bromdodecane, toluene, acetone, methanol, ethanol, *p*-toluene sulfonic acid and KHCO_3 were purchased from Merck Chemical Reagent Co. Ltd., 2,5-dimethoxybenzaldehyde was purchased from Alfa Easer Chemical Reagent Co. Ltd., and Pd/C (Karstedt's catalyst) was purchased from Aldrich Chemical Reagent Co. Ltd. All the reagents were used as received without further purification. All solvents were purified by standard methods.

2.2 5-(dimethoxy)-2-[[4-(dodecyloxy)phenyl]imino]methyl]benzene) (DDPIMB)

The DDPIMB was synthesized as shown in Fig. 1a. The new DDPIMB was prepared as described in previous studies [27, 28] by using *p*-toluene sulfonic acid (40 mg), catalyzed condensation of 6 mmol 4-dodecyloxyaniline with 5 mmol of 2,5-dimethoxybenzaldehyde in 50 ml toluene. The solution was refluxed for 6 h under an Ar atmosphere, and the imine compounds of DDPIMB were purified by several recrystallizations from acetone/ethanol. The obtained compound was in the form of beige crystals.

2.3 2,5-(dimethoxy)-2-[[4-(dodecyloxy)phenyl]imino]methyl]benzene (DDPIMB)

Yield: 1.60 g (%75), beige crystals

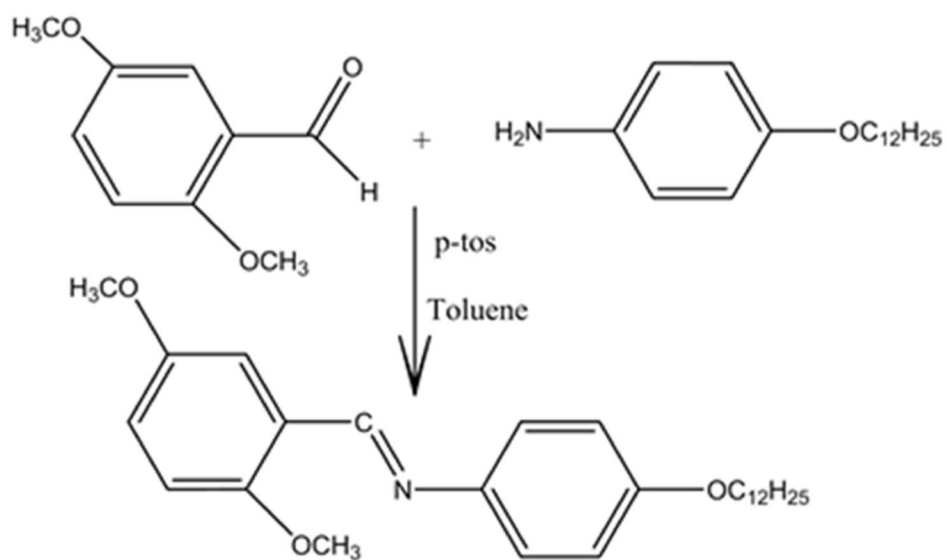
UV–VIS: λ (nm) = 349.3, FT-IR: ν (cm^{-1}) = 1624.4 ($-\text{C}=\text{N}$),

^1H -NMR (400 MHz, CDCl_3) δ (ppm) = 8.90 (*s*; HC=N), 7.30, 7.22, 7.01, 6.89 (*m*; 7H, ArH), 3.99 (*t*; 2H, $J \approx 6.5$ Hz; OCH_2), 3.75 (*t*; 6H, $J \approx 7.0$ Hz; OCH_3), 1.80–1.75 (*m*; OCH_2-CH_2), 1.40–1.20 (*m*; 18H, 9 CH_2), 0.85 (*t*; $J \approx 7.4$ Hz; CH_3).

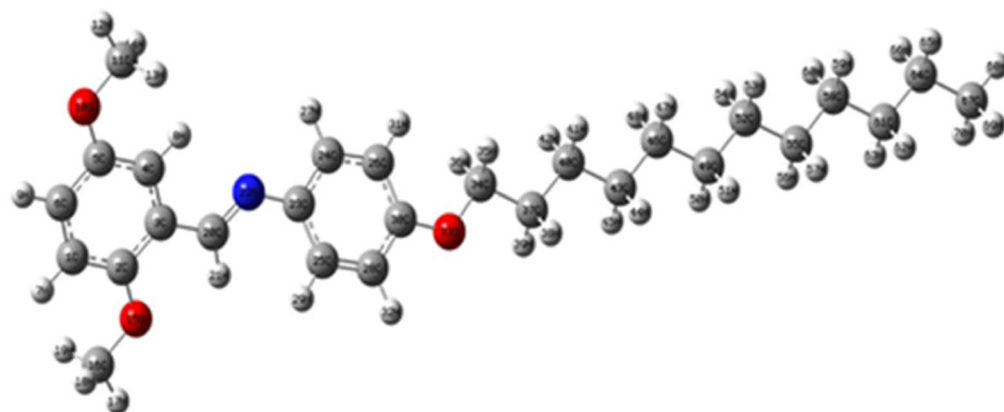
^{13}C -NMR (400 MHz, CDCl_3): δ (ppm) = 160.1, 159.8, 140.9, 123.5 (3 *s*; 5C, ArC), 159.9 (*d*, 1C, HC=N), 122.5, 115.8, 115.0, 107.5 (4*d*, 7C, ArCH), 68.6, (*t*, 1C, OCH_2), 59.2 (2 *s*; 2C, OCH_3), 31.2, 29.8, 29.4, 29.4, 29.4, 29.4, 29.4, 29.3, 29.3, 22.7 (10*t*, 10C, CH_2), 14.1, (*q*, 1C, CH_3).

2.4 Theoretical calculations

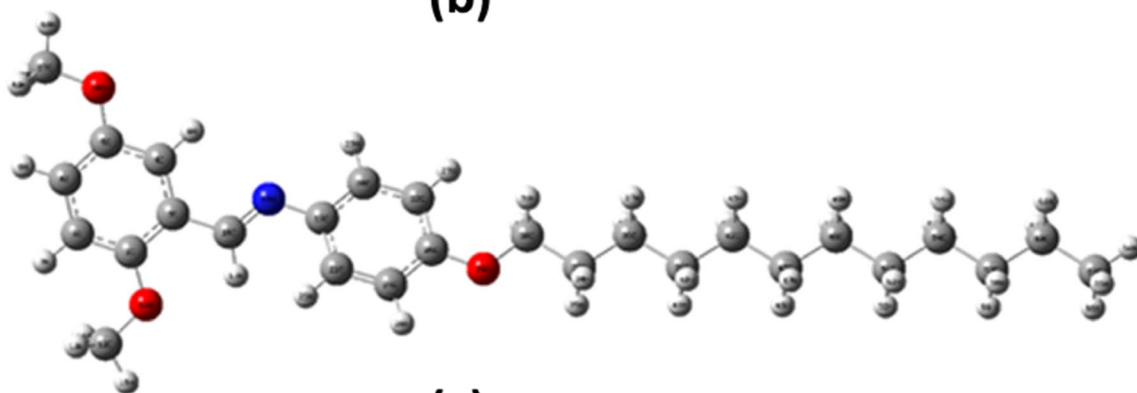
All calculations were made at DFT/B3LYP/6-311++G(d,p) level of theory [29–32] using Gaussian 09 software [33]. To find the most stable (or lowest energy) structure of the DDPIMB molecule, the cis–trans possible orientations were primarily optimized using the DFT/B3LYP/6-311++G(d,p) basis set. Calculated vibration frequencies are multiplied by 0.9682 [34], a global scaling factor for



(a)



(b)



(c)

Fig. 1 a Synthesis of b trans-orientation c cis-orientation optimized geometric structures of DDPIMB

B3LYP/6-311++G(d,p), making them more compatible with experimental results. These calculated vibration modes were assigned with the help of the VEDA 4 program [35]. ^1H and ^{13}C NMR isotropic chemical shifts were calculated in the chloroform solvent by the GIAO method [36, 37]. Many electronic properties of the title molecule in different solvents were obtained using the TD-DFT method. Moreover, NLO properties, dipole moments and molecular electrostatic potential (MEP) were investigated and discussed in detail.

3 Results and discussion

3.1 Spectroscopic characterization of DDPIMB with vibrational frequencies and infrared spectra

The O–CMe bonds of the two substituents of the phenyl group of the DDPIMB molecule had a trans–cis orientation. The optimized geometries of these orientations are shown in Fig. 1b, c, and the calculated energies are tabulated in Table 1.

The calculations show that the trans-orientation is the most stable. Therefore, all calculations were made for the trans-orientation on the DFT/B3LYP/6-311++G(d,p) level. The DDPIMB liquid crystal belonged to the point group symmetry C1 and had 204 normal vibration modes.

The measured, calculated FT-IR spectra and the correlation graph between them are given in Figs. 2 and 3, respectively. The theoretical wavenumbers and the potential energy distributions (PED values) of the vibrational modes for the liquid crystal are listed in Table 2 in comparison to the observed ones of this molecule. The FT-IR spectrum with a range of 700–4000 cm^{-1} , where functional groups are defined, can be seen in Fig. 2. The C=N characteristic band is observed in the range from 1672 to 1566 cm^{-1} [38]. In present study, the C=N stretching band appeared at 1624.4 cm^{-1} with medium intensity and this mode was computed 1618 cm^{-1} with 49% PED contribution with B3LYP/6-311++G(d,p) basis set. The benzylic C-H absorption band appeared at 3261 cm^{-1} . This band was calculated at 3113 cm^{-1} . The long chain alkyl group CH_3 symmetric and asymmetric stretching peaks appeared at 2959 cm^{-1} and 2917 cm^{-1} where the absorption band appeared at 2849 cm^{-1} with a medium peak. In the literature, the CH_3

Table 1 Calculated energies for two possible orientations of DDPIMB

Conformers	Energy (Hartree)
Cis orientation	– 1333.13086754
Trans orientation	– 1333.13243994

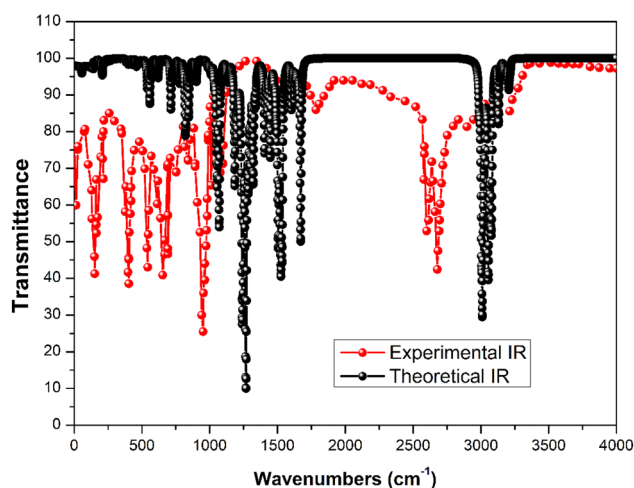


Fig. 2 Experimental and theoretical FT-IR spectra for DDPIMB

asymmetric stretching vibrations are observed at 2956 cm^{-1} , while the symmetric stretching vibrations are generally observed at 2873 cm^{-1} [39]. Theoretically, CH_3 asymmetric and symmetric modes were calculated at 2957 cm^{-1} (85% PED) and 2891 cm^{-1} (92% PED), respectively. The C–O stretching vibration was observed at 1129 cm^{-1} . The C–O stretching frequency observed as a sharp intensity band around 1275 cm^{-1} . This band was computed at 1278 cm^{-1} (92% PED). An absorption band obtained at 2956 cm^{-1} was due to the C–H stretching of the aromatic ring. The band at 1506 cm^{-1} was due to the C=C stretching frequency of the aromatic region. This mode calculated at 1595 cm^{-1} with 47% PED contribution by the B3LYP/6-311++ (d,p) method.

From the results, it is seen that all the spectroscopic data of the structure obtained with the proposed structure are fully compatible with each other. As can be seen in the correlation plot between experimental vibration modes and calculated vibration modes (Fig. 3), the correlation coefficient

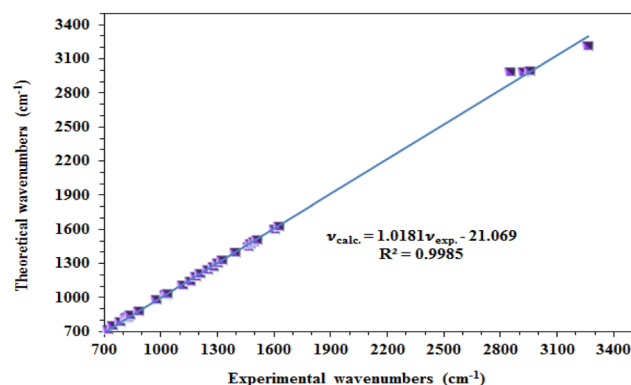


Fig. 3 Correlation plot of the theoretical and experimental FT-IR spectra (using data from Table 2) for DDPIMB

Table 2 Comparison of the selected experimental and theoretical vibrational frequencies of DDPIMB

Frequencies (cm ⁻¹)	B3LYP/6-311++G(d,p)	Experimental
δHCC (10), ΓHCCC (38)	713.84	718.56
ΓHCOC (18)	749.23	744.18
ΓHCCC (22), ΓHCOC (18)	781.54	785.77
ΓHCOC (19)	829.25	825.42
ΓHCOC (12)	879.23	882.49
υCC (52)	979.61	976.22
υOC (38), υCC (18)	1021.20	1022.74
υCC (60)	1033.46	1034.26
υCC (22), δCCC (34)	1107.14	1112.03
δHCO (30), ΓHCOC (23), ΓHCCC (20)	1150.92	1154.43
ΓHCCC (69)	1188.63	1184.73
υNC (21), δHCC (13)	1206.53	1208.92
υCC (12), υOC (27), δHCC (20)	1245.22	1246.04
δHCO (14), δHCC (11), ΓHCOC (13)	1270.82	
υCO (92)	1278.09	1275.40
υCC (43), δHCN (11)	1296.54	1297.12
ΓHCOC (14), ΓHCCC (38)	1309.16	
ΓHCOC (12), ΓHCCC (61)	1334.00	1323.06
ΓHCOC (74)	1379.97	1392.41
δHCH (73), ΓHCOC (24)	1444.24	1489.98
δHCC (73)	1464.06	1463.02
δHCC (12), δHCH (59)	1471.03	1472.46
δHCC (33)	1485.87	1406.40
υCC (47)	1595.15	1506.91
υNC (49), υCC (11)	1618.16	1624.42
υCH (92)	2891.43	2873.32
υCH (69)	2915.80	2917.87
υCH (85)	2957.76	2956.31
υCH (100)	3113.71	3261.98

υ: stretching, δ: in plane bending, γ: out of plane bending, Γ: torsion

is 0.9985. Environmental interactions neglected in the theoretical approach can create such small differences with experimental results.

3.2 Spectroscopic characterization with NMR

The ionic and reactive organic species can be identified by isotropic chemical shifts. Experimental and theoretical chemical shift values of DDPIMB are presented in Table 3. Similarly, the experimental ¹H and ¹³C NMR spectra of the molecule are presented respectively in Fig. 4a, b. The relationship graphs between measured and calculated chemical shifts are shown in Fig. 4c.

The square root correlation factor (R^2) for ¹³C was calculated to be 0.9685, and 0.9962 for ¹H. The experimental shifts of the sample prepared in the chloroform solvent

Table 3 Experimental and calculated chemical shifts (ppm) for DDPIMB

Atom	B3LYP/6311++G(d,p) Chloroform	Experimental Chloroform
C30	165.2	140.9
C2	160.3	160.0
C5	159.8	159.8
C20	156.9	159.9
C23	151.4	140.9
C24	133.3	123.5
C3	130.1	122.5
C6	125.9	115.8
C28	122.3	114.5
C25	121.3	123.5
C1	114.2	115.0
C26	112.9	114.5
C4	109.8	107.5
C34	71.2	68.8
C11	54.9	59.2
C16	54.7	59.2
C61	37.6	29.4
C58	36.7	29.4
C52	36.7	29.4
C46	36.4	29.3
C55	36.1	29.4
C49	35.9	29.4
C43	35.5	29.8
C37	34.0	31.2
C40	30.5	29.3
C64	28.3	22.7
C67	15.4	14.1
H21	9.32	8.9
H8	7.94	7.30
H29	7.57	7.22
H27	7.51	7.22
H9	7.18	6.89
H32	7.14	7.01
H31	6.93	7.01
H7	6.79	6.89
H17	4.12	3.75
H12	3.98	3.75
H35	3.80	3.99
H36	3.80	3.99
H18	3.73	3.75
H13	3.71	3.75
H19	3.68	3.75
H14	3.67	3.75
H38	1.80	1.75
H39	1.79	1.75
H44	1.35	1.2
H45	1.33	1.2
H42	1.29	1.4

Table 3 (continued)

Atom	B3LYP/6311++G(d,p)	Experimental
Solvent	Chloroform	Chloroform
H66	1.29	1.2
H65	1.28	1.2
H59	1.27	1.2
H53	1.27	1.2
H42	1.26	1.4
H47	1.26	1.2
H48	1.25	1.2
H51	1.24	1.2
H54	1.23	1.2
H56	1.23	1.2
H50	1.22	1.25
H60	1.21	1.2
H57	1.21	1.2
H62	1.17	1.2
H63	1.15	1.2
H68	1.07	0.85
H69	0.75	0.85
H70	0.73	0.85

were observed as follow: $^1\text{H-NMR}$ spectrum; imine proton at 8.9 ppm, ring protons at 6.9–7.3 ppm, lateral $-\text{O}-\text{CH}_3$ protons at 3.75 ppm, $-\text{O}-\text{CH}_2$ protons 3.9, $-\text{CH}_2$ protons 1.75–1.2 ppm, $-\text{CH}_3$ protons 0.85 ppm. The theoretical $^1\text{H-NMR}$ chemical shifts were calculated in the range of 0.73–9.32 ppm. It was observed that there was a match between the theoretical and experimental results except for the overestimations. These overestimations could have occurred for two reasons. The first one is that theoretical calculations were made in the gas phase, while experimental measurements were taken in the solid phase. Secondly, electronegative atoms such as oxygen and nitrogen affect their surrounding atoms, and a higher ppm value also shows shifts.

The ^{13}C NMR spectrum for the title molecule was as $\text{C}=\text{N}$ imine carbon at 159.9 ppm, ring carbons at 160.1, 159.8, 140.9, 123.5, 122.5, 115.8, 115.0, 107.5, $\text{O}-\text{CH}_2$ at 68.6 ppm, $\text{O}-\text{CH}_3$ at 59.2 ppm, $\text{O}-\text{CH}_2-\text{CH}_2$ at 31.2 ppm, $-\text{CH}_2$ 29.8–29.4 and the $\text{C}-\text{CH}_3$ structure peaked at 14.1 ppm. The theoretical $^{13}\text{C-NMR}$ chemical shifts were obtained in the range of 15.4–165.2 ppm. Looking at the Table 3, the dodecyloxy-terminated carbon atoms in the chain provided higher ppm-values due to the electronegative H atoms attached to them.

3.2.1 NLO (non-linear optical) analysis

NLO materials have wide production areas such as laser technology, optical switching, photonic devices, optical sensors, screens, and data storage [41–43]. Useful and reliable results

are obtained in the search of new nonlinear materials through quantum computing approaches. In this respect, DFT-based methods are the best in terms of computation time and accuracy [44]. To investigate the electrical and optical responses of the studied liquid crystal, electrical dipole moment (μ), Hyper-polarizability (β) and polarizability (α) values from NLO properties were investigated using DFT/B3LYP/6-311++G(d,p) theory. The values of average polarizability (α), anisotropy of polarizability ($\Delta\alpha$), average molecular hyperpolarizability (β) and total dipole moment were obtained with the help of below equations and presented in Table 4.

$$\alpha_{tot} = \frac{1}{3}(\alpha_{xx} + \alpha_{yy} + \alpha_{zz}) \quad (1)$$

$$\Delta\alpha = \frac{1}{\sqrt{2}} \left[(\alpha_{xx} - \alpha_{yy})^2 + (\alpha_{yy} - \alpha_{zz})^2 + (\alpha_{zz} - \alpha_{xx})^2 + 6\alpha_{xz}^2 + 6\alpha_{xy}^2 + 6\alpha_{yz}^2 \right]^{\frac{1}{2}} \quad (2)$$

$$\langle\beta\rangle = \left[(\beta_{xxx} + \beta_{xyy} + \beta_{xzz})^2 + (\beta_{yyy} + \beta_{yzz} + \beta_{yxx})^2 + (\beta_{zzz} + \beta_{zxx} + \beta_{zyy})^2 \right]^{\frac{1}{2}} \quad (3)$$

$$\mu_{tot} = \left(\mu_x^2 + \mu_y^2 + \mu_z^2 \right)^{\frac{1}{2}} \quad (4)$$

It is important to interpret the optoelectronic properties of NLO properties of materials such as optically active liquid crystals. For a molecule to behave like a good NLO material, the first order hyperpolarizability, dipole moment and polarity must be large. The magnitude of these values is often interpreted by comparing them with the values of Urea. Here, the values of β_{tot} and $\Delta\alpha$ were calculated as 35.14×10^{-30} esu and 161.12×10^{-24} esu, respectively. These values for urea were as: $\beta_{tot} = 0.37 \times 10^{-30}$ esu and $\Delta\alpha = 3.83 \times 10^{-24}$ esu [45]. It is seen that the first order hyperpolarizability value of the liquid crystal was approximately 94 times higher than that of Urea, and similarly, the mean polarizability was about 42 times larger. With these results, it can be said that the DDPIMB liquid crystal is a high potential candidate molecule for future NLO applications.

3.3 Electronic properties

3.3.1 UV-Vis spectral analysis

The interaction of the liquid crystal molecule with light is important for understanding its electronic structure and designing new optical devices. In small and high absorption liquid crystals, elementary charge and excitation

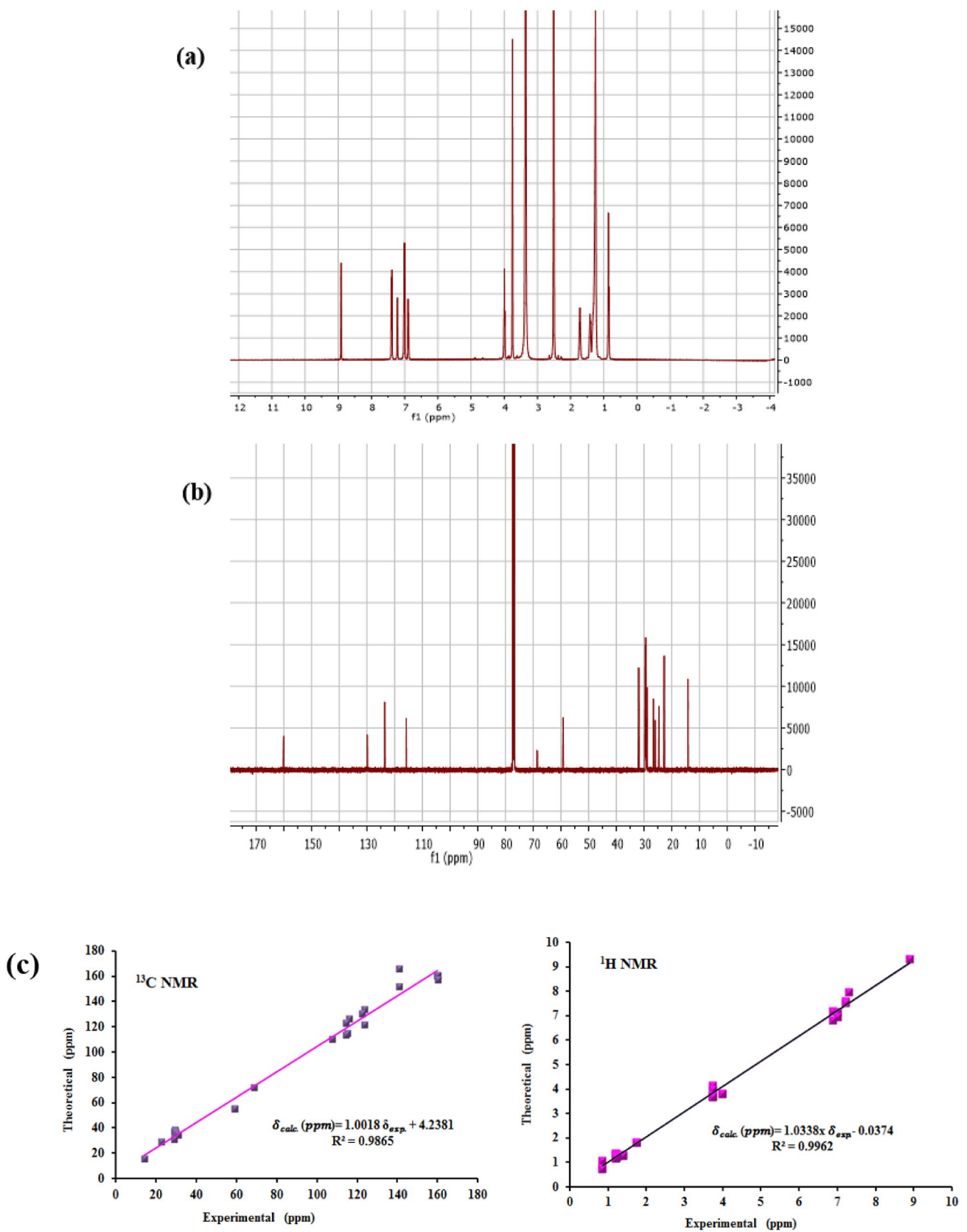


Fig. 4 a The ^1H -NMR b The ^{13}C -NMR spectrum c Correlation graphics between the experimental and theoretical NMR chemical shifts (using data from Table 3) for DDPIMB

Table 4 The dipole moments, polarizability (a.u.), average polarizability ($\times 10^{-24}$ esu), anisotropy of polarizability ($\times 10^{-24}$ esu) and first hyperpolarizability ($\times 10^{-33}$ esu) of DDPIMB

μ_x	0.58	β_{xxx}	-35632.56
μ_y	-0.56	β_{xxy}	3118.53
μ_z	-0.62	β_{xyy}	1143.51
μ_{tot}	1.08	β_{yyy}	-441.45
α_{xx}	88.84	β_{xxz}	-3782.43
α_{xy}	-0.36	β_{xyz}	148.52
α_{yy}	50.63	β_{yyz}	51.46
α_{xz}	2.69	β_{xzz}	-309.01
α_{yz}	-0.90	β_{yzz}	58.81
α_{zz}	35.24	β_{zzz}	-281.63
α_{total}	58.23	β_x	-34798.06
$\Delta\alpha$	161.12	β_y	2735.89
		β_z	-4012.60
		β	35135.32

energy analysis can be done by quantum chemical methods. As a result of the calculations, the applicability of such molecules on flexible screens and photovoltaic devices is determined [46]. The UV–Vis spectral parameters were calculated using the method/basis set TD-DFT-B3LYP/6-311++G(d,p) in acetone, chloroform, water and gas phases as shown in Table 5. From the table, it is seen that the electronic transition from the ground state to the first excited state was from HOMO (116) to LUMO (117). There is also a transition to the absorption maxima that has the highest oscillator strength at the same time. The lowest excitation energy for the electronic transition from ground to excited state is calculated as 3.22 eV and is smaller than 3.73 eV energy gap. The electrical band gap, which is the energy difference between HOMO and LUMO levels, and the optical band gap, which is the excitation energy for transitions between vertical bands, are different energies [47]. Here, the 3.73 eV energy value calculated using the TD-DFT method shows the electrical band range and the 3.22 eV energy value shows the optical band range. The electronic band gap is known to be larger than the optical band gap, and this difference value is called reorganization energy [48]. Lower reorganization energy values mean higher charge transfer rate [49, 50]. This small reorganization energy of 0.51 eV indicates that the DDPMI has a high charge transfer rate and can be used as a charge transfer material.

Figure 5a shows the calculated absorption spectra of the liquid crystal molecule defining UV–VIS spectral assignments using the TD-DFT method in acetone, chloroform, water, and gas phases. A four-band structure was observed with the absorptions of 260, 288, 346 and 375–385 nm for all solvents. From these results, it may be stated that the absorption energy of the molecule is affected by the solvent environment except for the gas phase.

Table 5 The computed absorption wavelengths, excitation energies, absorbance and oscillator strengths of DDPIMB

λ (nm)	E (eV)	f	Transition
<i>Acetone</i>			
385	3.22	0.6850	H→L
345	3.59	0.0448	H-1→L
287	4.32	0.2057	H-4→H-4→L, H-2→L, H-1→L, H→L+1
282	4.39	0.0178	H-1→L+1, H→L+1
261	4.74	0.0459	H-4→L, H→L+1, H→L+2, H→L+3
259	4.77	0.0840	H-3→L, H→L+2
<i>Chloroform</i>			
341	3.63	0.7656	H→L
304	4.08	0.0343	H-1→L
266	4.65	0.2826	H-4→L, H-3→L, H-2→L, H-1→L
261	4.74	0.0410	H-2→L, H-1→L+5, H→L+5
231	5.36	0.0085	H-3→L, H-2→L, H-1→L+2, H→L+1
230	5.38	0.0106	H-4→L, H-1→L, H-1→L+11, H→L+1
<i>Gas</i>			
375	3.30	0.6107	H→L
340	3.64	0.0149	H-4→L, H-1→L
288	4.30	0.2126	H-4→L, H-3→L, H-2→L, H-1→L
282	4.39	0.0079	H-2→L, H→L+1
266	4.66	0.0006	H-1→L+3, H→L+2, H→L+3
<i>Water</i>			
385	3.22	0.6783	H→L
346	3.58	0.0476	H-1→L
287	4.32	0.2033	H-4→L, H-2→L, H-1→L
282	4.39	0.0189	H-1→L+1, H→L+2
261	4.74	0.0450	H-4→L+1, H→L+1, H→L+2, H→L+3
259	4.77	0.0832	H-3→L, H→L+1

3.4 Fundamental optical parameters

Absorbance is a key parameter for photonic and optoelectronic devices. It provides important information about the electronic structure and optical behavior of the material. Figure 5b indicates the experimental absorbance spectra of DDPIMB. The DDPIMB liquid crystal displayed the maximum absorbance peak at 355 nm, and its absorbance remained almost constant after 430 nm.

The fundamental parameters such as absorption band edge, optical band gap (E_g) and refractive index (n) of the liquid crystal were obtained.

The absorption band edge of the liquid crystal was calculated from the $dT/d\lambda$ curves vs. wavelength (λ) as seen in Fig. 6 using the methods described in the literature [51, 52]. As seen in Fig. 5b, the maximum peak (λ_{max}) position

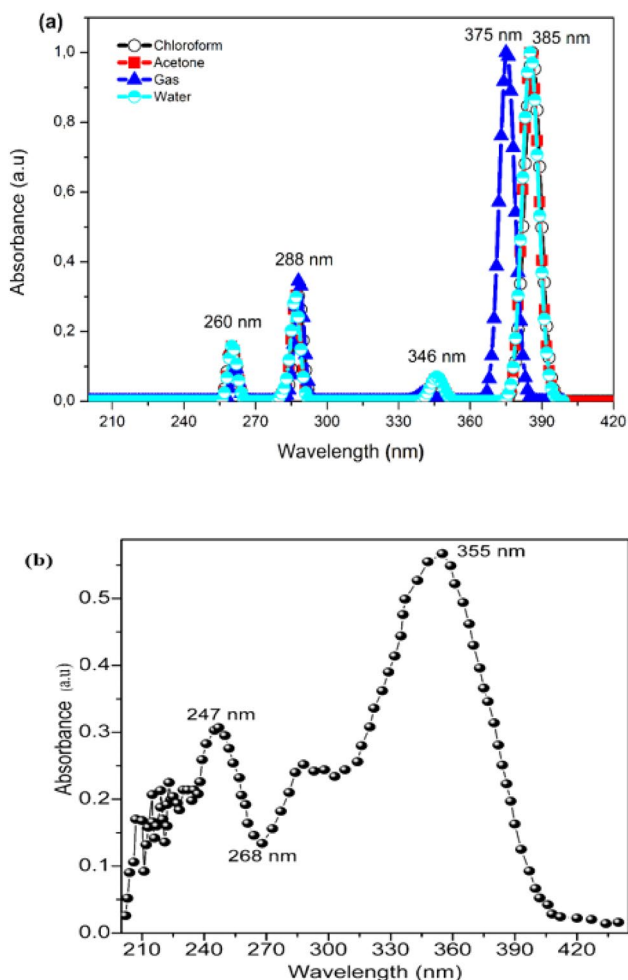


Fig. 5 The a theoretical b experimental absorbance spectra of DDPIMB

corresponds to the absorption band edge was found as 3.039 eV using the formula $E_{b-e} = 1240/\lambda_{max}$.

The optical band gap of the liquid crystal was obtained from the well-known Tauc method [53],

$$(\alpha h\nu) = A(h\nu - E_g)^n \tag{5}$$

where α is the absorption coefficient, A is a constant, $h\nu$ is the photon energy, and n is a parameter. The $(\alpha h\nu)^2$ vs. photon energy (E) plot of the DDPIMB liquid crystal is shown in Fig. 7. The optical band gap of DDPIMB was found to be 3.136 eV. The obtained results suggested that the liquid crystal is a material with an optical band gap range for the production and application of optoelectronic devices such as diodes, photodiodes, and sensors. On the other hand, the optical band gap and the absorbance band edge of the liquid crystal were close to each other.

Refractive index (n) is the ratio of the speed of light in one medium to another. Furthermore, it is an essential

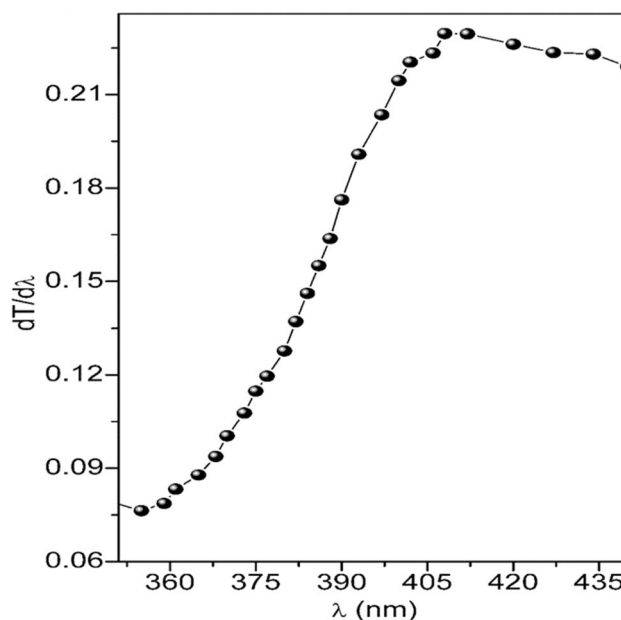


Fig. 6 The experimental $dT/d\lambda$ curve vs. wavelength (λ) of DDPIMB

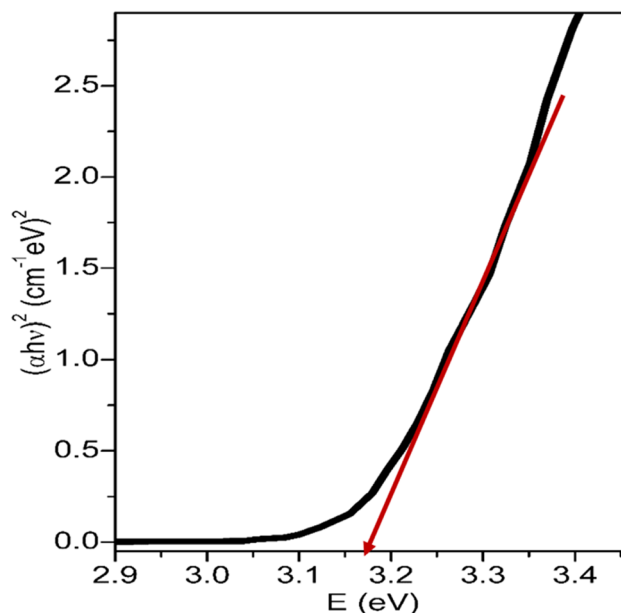


Fig. 7 The experimental $(\alpha h\nu)^2$ plot vs photon energy (E) of the DDPIMB

property since ions and materials in the local area are closely related to electronic polarization [54]. Thin film materials with a refractive index greater than 1.65 are used to increase the performance of optical and photovoltaic devices such as solar cells due to their high refractive indexes [55, 56]. In this context, the refractive index values of the optical crystal were calculated according to the optical band gap with different relationships such as Ravindra,

Reddy, Herve-Vandamme, Kumar-Singh and Moss [57]. The respective refractive index values of the liquid crystal were found to be 2.140, 2.730, 2.289, 2.329 and 2.346 for the aforementioned relations. All these relations give results that are quite compatible with experimental results. In particular, the Reddy correlation is a modification of the Moss correlation, giving results perfectly compatible with the experimental results of materials with an energy range of $1.1 \text{ eV} < E_g < 6.2 \text{ eV}$. [57]. Although calculated refractive index values are close to each other, we can say that 2.730 refractive index is the most suitable result for DDPIMB.

3.5 Analysis of frontier molecular orbitals and physicochemical properties

The lowest unoccupied molecular orbital (LUMO) known to have the ability to receive electrons and the highest occupied molecular orbital (HOMO) known to have the ability to give electrons are important orbitals. This is because the difference between E_{HOMO} and E_{LUMO} can explain the

electrical and optical parameters of the molecule, its chemical reactivity and its stability [58]. The frontier molecular orbitals (HOMO and LUMO) energies were calculated by the TD-DFT/B3LYP/6-311++G (d,p) method in acetone, chloroform solutions and gas phase. The HOMO–LUMO forms of the liquid crystal in the gas phase are given in Fig. 8. Additionally, the HOMO–1 and LUMO+1 orbitals, which were the closest to the HOMO and LUMO orbitals, are also provided in Fig. 8. The red and green colors indicate the positive and negative phases of the molecular orbitals, respectively. The HOMO orbitals or valance band and LUMO orbitals or conduction band spread over the molecule except for the dodecyloxy and methyl groups. Furthermore, in the molecular crystal, it was seen that the dodecyloxy side chain did not affect its HOMO–LUMO orbitals or band structure. The energy gap (E_g) which is the energy difference between the HOMO and LUMO is a critical parameter in measuring electron conductivity and molecular reactivity. As shown in Table 6, this value was 3.73 eV in the gas phase and 3.71 eV in the acetone and chloroform solvents. This

Fig. 8 The calculated frontier molecular orbitals of DDPIMB obtained with the B3LYP/6-311++G(d,p) level

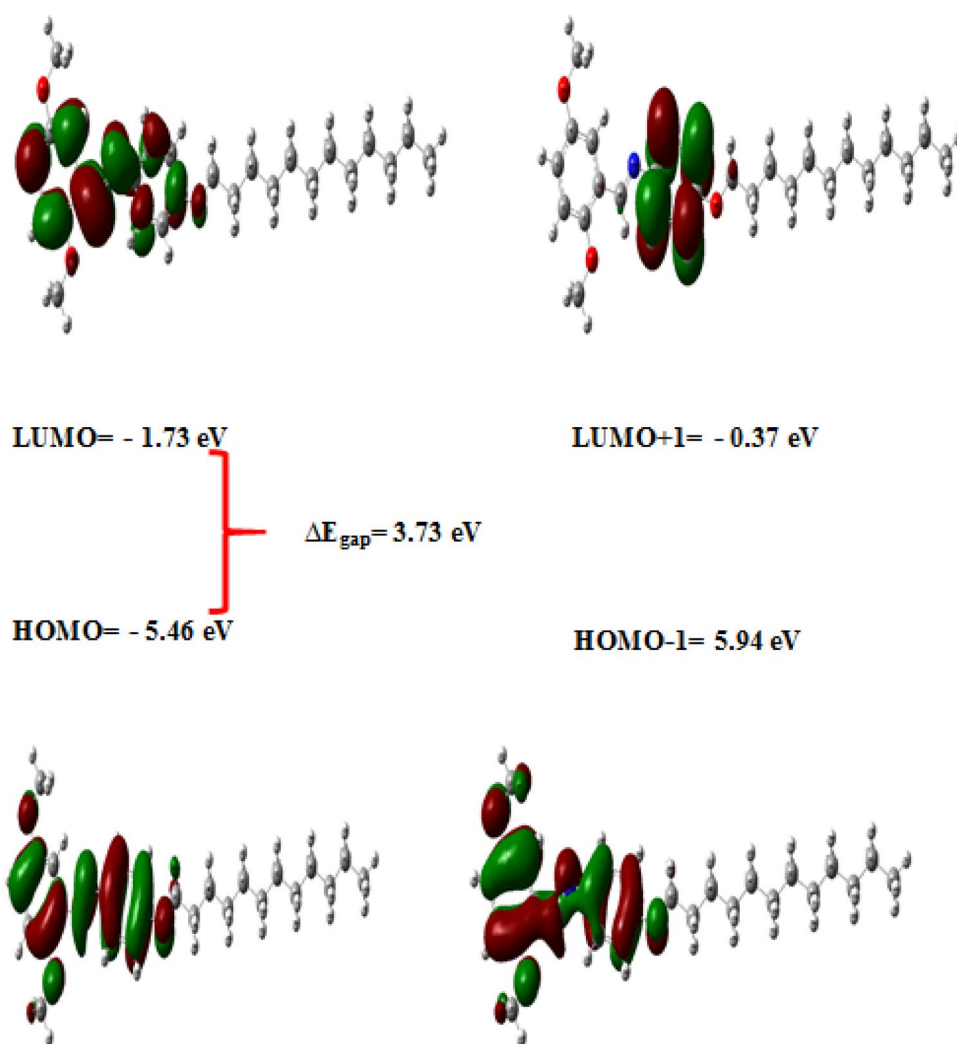


Table 6 The energy values of DDPIMB molecules calculated using the TD-DFT/B3LYP method in the 6-311++G(d,p) basis set

	Acetone	Gas	Chloroform
E_{total} (Hartree)			
E_{HOMO} (eV)	− 5.72	− 5.46	− 5.65
E_{LUMO} (eV)	− 2.01	− 1.73	− 1.93
$E_{\text{HOMO}-1}$ (eV)	− 6.18	− 5.94	− 6.11
$E_{\text{LUMO}+1}$ (eV)	− 0.65	− 3.37	− 0.57
$E_{\text{HOMO}-1-\text{LUMO}+1}$ gap (eV)	− 5.53	− 5.57	− 5.54
$E_{\text{HOMO}-\text{LUMO}}$ gap (eV)	3.71	3.73	3.71
Chemical hardness (h)	− 1.85	− 1.87	− 1.86
Electronegativity (χ)	3.87	3.60	3.79
Chemical potential (μ)	− 3.87	− 3.60	− 3.79
Electrophilicity index (ω)	− 4.03	− 3.47	− 3.87

result shows that DDPIMB has higher conductivity in acetone and chloroform. Furthermore, the 3.71 eV gap (336 nm) is in the UV-A region considering light absorption, and this liquid crystal can easily be polarized with this low energy range and easily interact with other molecules with minimal energy. The calculated chemical hardness, electronegativity, chemical potential and electrophilicity index values for all solvents are given in Table 6.

3.6 Molecular electrostatic potential

Molecular MEP surface analysis is performed to investigate regions with positive, negative and neutral electrostatic potential in the molecule based on color grading [59, 60]. Thus, the molecule is examined in terms of physicochemical, nucleophilic and electrophilic. In this visual presentation of chemical activity, the red (negative) surface of MEP indicated electrophilic reactivity and the electron-donating reaction, while the blue (positive) surface is pertinent to nucleophilic reactivity and the electron-accepting reaction. MEP

surface determined using the B3LYP/6-311++G(d,p) basis set and are presented in Fig. 9. On the MEP surface, where different colors represent different electrostatic potential values, a color spectrum from red to blue was used. Figure 9 shows that regions with negative potential concentrate on O atoms, whereas regions with positive potential are concentrated on H atoms.

3.7 Mesomorphic properties

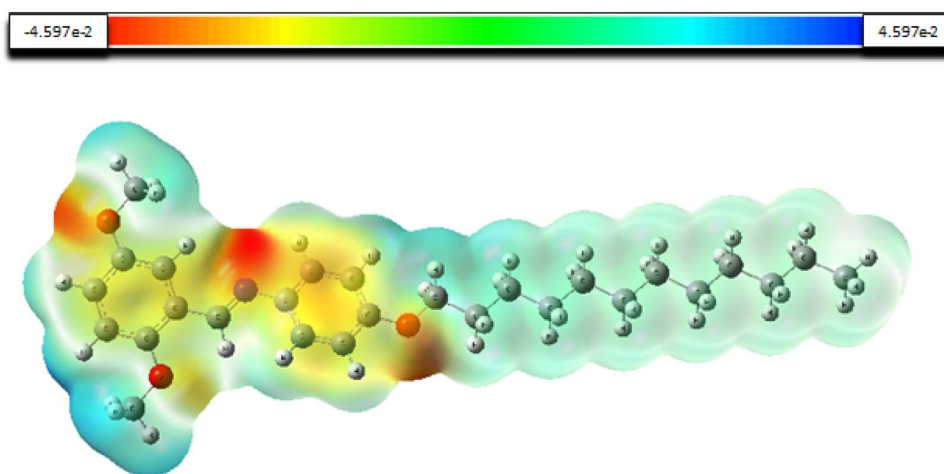
The mesogenic properties of DDPIMB were investigated by PM using a heating and cooling stage. The phase transition temperatures and enthalpy values were measured by DSC thermal analysis. The texture of the smectic mesophase of DDPIMB are given in Fig. 10.

The DSC thermograms of the investigated compound DDPIMB are shown in Fig. 11. The compound DDPIMB shows the enantiotropic smectic mesophase which is a range of a smectic X phase. The texture of the smectic X is undefined. The DSC thermogram of DDPIMB shows two endothermic peaks at 54.2 °C and 80.4 °C in the heating cycle and two exothermic peaks at 52.0 °C and 76.2 °C in the cooling cycle. The two endothermic peaks showed the crystal (Cr)→mesophase (SmX)→isotropic(I) phase transitions, respectively. The two exothermic peaks defined the I→mesophase (SmX)→Cr phase transitions. The transition temperatures and corresponding enthalpy values for DDPIMB are shown in Table 7.

4 Conclusion

In this study, the 2,5-(dimethoxy)-2-[[4-(dodecyloxy)phenyl]imino]methyl]benzene (DDPIMB) calamitic liquid crystal was synthesized and characterized by FT-IR ^1H - ^{13}C NMR and UV-vis spectroscopy techniques. The phase behavior of the thermotropic enantiotropic liquid crystal

Fig. 9 The Molecular electrostatic potential (MEPs) map of DDPIMB at the B3LYP/6-311++G (d,p) level



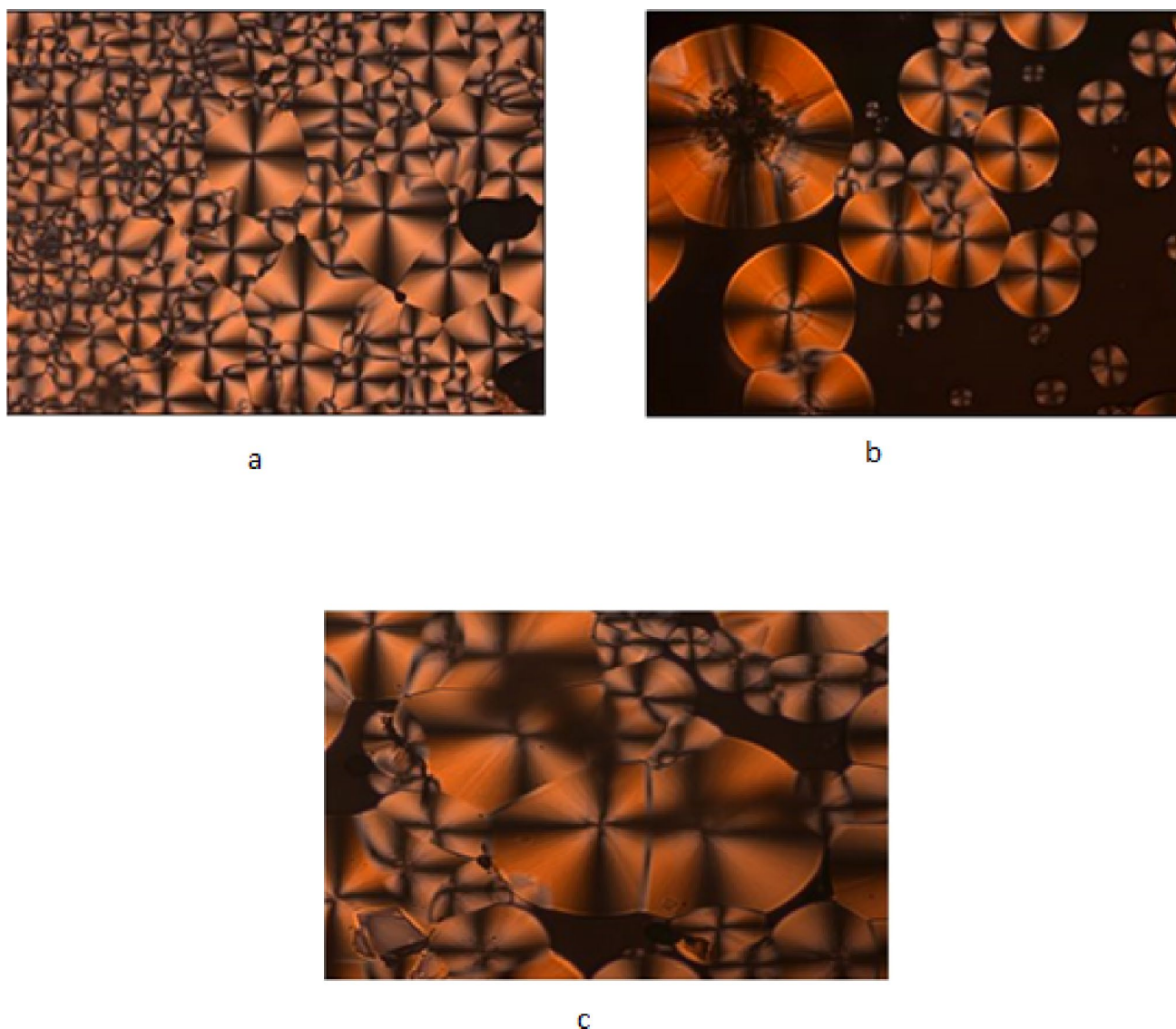


Fig. 10 PM photomicrographs as observed on cooling for **a** the SmX mesophase of DDPIMB at $T=55\text{ }^{\circ}\text{C}$; **b** the SmX mesophase of 1b at $T=58\text{ }^{\circ}\text{C}$ and **c** the SmX mesophase of 1b at $T=64\text{ }^{\circ}\text{C}$

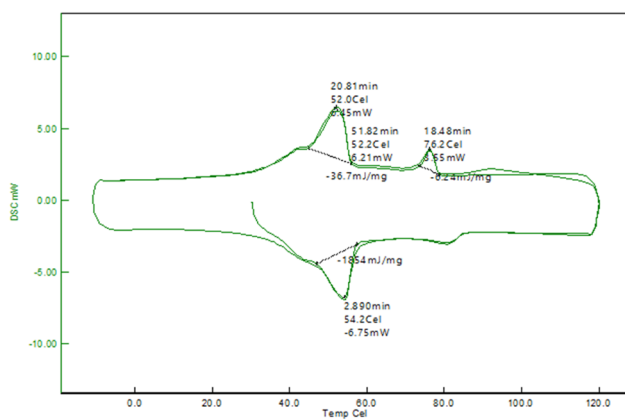
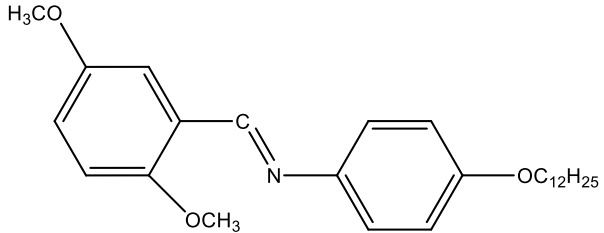


Fig. 11 DSC thermogram of the investigated compound DDPIMB in heating and cooling cycle

DDPIMB was investigated by PM and DSC. DDPIMB showed the enantiotropic smectic X mesophase which had an undefined texture. Theoretically, vibrational, electrical, and nonlinear optical properties were analyzed using the DFT approach. Both experimental and theoretical methods showed that the compound was successfully synthesized, and it was also found that the theoretical and experimental results were consistent. TD-DFT calculations were performed to obtain UV–VIS spectral analysis of the synthesized liquid crystal. Frontier Molecular Orbital Analysis and physicochemical properties were calculated by the same theory of level in acetone, chloroform, and gas phases. The TD-DFT calculations showed that the HOMO (MO:116)-LUMO (MO:117) transition at a wavelength of 341 nm was at the highest oscillator strengths of $f=0.7656$ in the

Table 7 Phase transition temperatures T ($^{\circ}\text{C}$) and associated transition enthalpies ΔH (kJ mol^{-1}) of DDPIMB

	
Compound	T $^{\circ}\text{C}$ (ΔH mJ/mg)
DDPIMB	K 52.0 (36.7) SmX 76.2 (6.24) Iso
^a Cr: crystalline, Sm: smectic, and Iso: isotropic liquid phase; transition temperatures and enthalpy values were determined by DSC (Perkin-Elmer DSC-7; heating rates 10 K min^{-1}).	

chloroform solvent. It was also seen that the results in the chloroform solvent were compatible with the experimental results. The header molecule's hyper polarizability, electric dipole moment and polarizability were obtained from the frequency output file. The first-order hyperpolarizability of the liquid crystal was calculated to be 94 times higher than that of urea ($\beta = 0.37 \times 10^{-30}$ esu), and the mean polarizability was calculated to be 42 times greater than that of urea ($\Delta\alpha = 3.83 \times 10^{-24}$). The results showed that this liquid crystal could be a good NLO material. Furthermore, the fundamental optical parameters of the liquid crystal were obtained by the semi-empirical method. The DDPIMB liquid crystal, which has a 3.136 eV optical band gap, is thought to be a material with a band gap spacing suitable for the production and application of optoelectronic devices such as diodes, photodiodes and sensors. It has the feature of being a charge transfer material with its 0.51 eV reorganization energy. The results that were obtained suggested that the liquid crystal was a material with a suitable optical band gap range for production and application of optical and optoelectronic devices.

Acknowledgements This research was supported by TUBITAK. Project Number: 1919BO11602561.

References

- N. Nandi, H.K. Singh, S.K. Singh, B. Singh, *Liq. Cryst.* **40**, 884–889 (2013)
- M. Roychoudhury, P.K. Gaurav, R. Manohar, A.K. Prajapati, *Mol. Cryst. Liq. Cryst.* **537**, 3 (2011)
- J. Herman, E. Dmochowska, M. Czerwinski, *J. Mol. Liq.* **271**, 353 (2018)
- Ç. Yörür, A. Nesrullajev, B. Bilgin-Eran, *Mol. Phys.* **105**, 23 (2007)
- R.J. Carlton, J.T. Hunter, D.S. Miller, R. Abbasi, P.C. Mushenheim, L.N. Tan, N.L. Abbott, *Liq. Cryst. Rev.* **1**, 29 (2015)
- M.R. Darla, S. Varghese, *Liq. Cryst.* **39**, 1 (2012)
- G. Karanlık, H. Ocak, B.B. Eran, *J. Mol. Liq.* **275**, 567–577 (2019)
- S. Mutlu Yanic, F. Cakar, H. Ocak, F. Karaman, O. Cankurtaran, B.B. Eran, *J. Chem. Eng. Data* **64**, 3 (2019)
- H. Ocak, B. Bilgin-Eran, M. Prehm, S. Schymura, J.P.F. Lagerwall, C. Tschierske, *Soft Matter* **7**, 8266 (2011)
- H. Ocak, B. Bilgin-Eran, M. Prehm, C. Tschierske, *Soft Matter* **8**, 7773 (2012)
- S. Mutlu Yanic, H. Ocak, F. Cakar, B. Bilgin-Eran, D. Guzeller, O. Cankurtaran, *Optoelectron. Adv. Mater. Rapid Commun.* **11**, 77 (2017)
- M.G. Reddy, N.P. Lobo, T. Narasimhaswamy, *Liq. Cryst.* **43**, 896 (2016)
- V.S. Sharma, R.B. Patel, *Mol. Cryst. Liq. Cryst.* **648**, (2017)
- C.C. Huang, C.C. Hsu, L.W. Chen, Y.L. Cheng, *Soft Matter* **10**, 9343 (2014)
- B.N. Veerabhadraswamy, D.S.S. Rao, C.V. Yelamaggad, *J. Phys. Chem. B* **119**, 12 (2015)
- R. Nandi, H.K. Singh, S.K. Singh, D.S.S. Rao, K. Prasad, B. Singh, R.K. Singh, *J. Liq. Cryst.* **44**, 1185 (2017)
- S. Kumar, *Liquid Crystal: Experimental Study of Physical Properties and Phase Transitions* (Cambridge University Press, Cambridge, 2001), pp. 65–93
- R. Nandi, K. Vikram, S.K. Singh, B. Singh, R.K. Singh, *Vib. Spec.* **69**, 40 (2013)
- R. Nandi, S.K. Singh, H.K. Singh, R.D. Shankar, P.S. Krishna, B. Singh, R.K. Singh, *J. Raman Spectrosc.* **47**, 9 (2016)
- R. Nandi, H.K. Singh, S.K. Singh, B. Singh, R.K. Singh, *Spectrochim. Acta A* **128**, 248 (2014)
- S.K. Saha, J. Deb, U. Sarkar, M.K. Paul, *J. Liq. Cryst.* **44**, 14 (2017)
- K. Druzbecki, E. Mikuli, *Spectrochim. Acta A* **77**, 402 (2010)

23. D.D. Sarkar, R. Deb, N. Chakraborty, G. Mohiuddin, R.K. Nath, V.S.R. Nandiraju, *Liq. Cryst.* **39**, 8 (2013)
24. D. Pegu, J. Deb, C. Van Alsenoy, U. Sarkar, *Spectrosc. Lett.* **50**, 4 (2017)
25. V. Barone, A. Baiardi, M. Biczysko, J. Bloino, C. Cappelli, F. Lipparini, *Phys. Chem. Chem. Phys.* **14**, 12404 (2012)
26. V. Barone, M.B. Biczysko, *J. Phys. Chem. Chem. Phys.* **16**, 1759 (2014)
27. N. Yilmaz-Canli, B. Bilgin-Eran, A. Nesrullajev, *J. Mol. Struct.* **990**, 79 (2011)
28. A. Nesrullajev, B. Bilgin-Eran, *Cryst. Res. Technol.* **43**, 3 (2008)
29. W. Kohn, L.J. Sham, *Phys. Rev.* **140**, A1133 (1965)
30. A.D. Becke, *Phys. Rev. A.* **38**, 3098 (1988)
31. S.H. Vosko, L. Vilk, M. Nusair, *Can. J. Phys.* **58**, 1200 (1980)
32. C. Lee, W. Yang, R.G. Parr, *Phys. Rev. B* **37**, 785 (1988)
33. M.J. Frisch, H.P. Hratchian, R.D. Dennington II, T.A. Keith, J. Millam, B. Nielsen, A.J. Holder, J. Hiscocks, Gaussian, Inc., GaussView Version 5.0.8 (2009)
34. J.P. Merrick, D. Moran, L. Radom, *J. Phys. Chem. A* **111**, 11683 (2007)
35. M.H. Jamroz, *Spectrochim. Acta A* **14**, 220 (2013)
36. R. Ditchfield, *J. Chem. Phys.* **56**, 5988 (1972)
37. K. Wolinski, J.F. Hinton, P. Pulay, *J. Am. Chem. Soc.* **112**, 8251 (1990)
38. H. Saral, Ö. Özdamar, I. Ucar, Y. Bekdemir, M. Aygün, *J. Mol. Struct.* **1103**, 5 (2016)
39. B.H. Stuart, *Infrared Spectroscopy: Fundamentals and Applications*, (Wiley, Hoboken, 2004), p. 139
40. E. Tanış, E.B. Sas, M. Kurban, M. Kurt, *J. Mol. Struct.* **1154**, 301 (2018)
41. S. Muthu, J. Uma Maheswari, *Spectrochim. Acta A* **92**, 154 (2012)
42. K. Govindarasu, E. Kavitha, *Spectrochim. Acta A* **122**, 130 (2014)
43. K. Govindarasu, E. Kavitha, N. Sundaraganesan, *Spectrochim. Acta A* **133**, 417 (2014)
44. O. Christiansen, J. Gauss, J.F. Stanton, *Chem. Phys. Lett.* **305**, 147 (1999)
45. K.M. Hijas, S.M. Kumar, K. Byrappa, T.G. Jeyaram, R. Nagalakshmi, *J. Mol. Struct.* **1155**, 249 (2018)
46. P.L. Praveen, D.S. Ramakrishna, P.O. Durga, *Mol. Cryst. Liq. Cryst.* **643**, 76 (2017)
47. J.R. Reynolds, B.C. Thompson, T.A. Skotheim, *Conjugated Polymers Properties, Processing and Applications*, 4th edn. (CRC Press, New York, 2019), pp. 61
48. P. Javier, C. Enrique, W.C. Alex, A. Javier, F.H. Susana, B.P. Martin, *J. Chem. Phys.* **139**, 224103 (2013)
49. A. Chandekar, J.E. Whitten, *Synth. Met.* **150**, 259 (2005)
50. S. Mohakud, A.P. Alex, S.K. Pati, *J. Phys. Chem. C* **114**, 20436 (2010)
51. B. Gündüz, *Polym. Bull.* **72**, 3241 (2015)
52. B. Gündüz, *Opt. Mater.* **36**, 425 (2013)
53. J. Tauc, A. Menth, *J. Non-Cryst. Solids* **8**, 569 (1972)
54. S.W. Xue, X.T. Zu, W.L. Zhou, H.X. Deng, X. Xiang, L. Zhang, H. Deng, *J. Alloys Compd.* **448**, 21 (2008)
55. M. Oubaha, S. Elmaghrum, R. Copperwhite, B. Corcoran, C. McDonagh, A. Gorin, *Opt. Mater.* **34**, 1366 (2012)
56. C. Leguijt, P. LokIgen, J.A. Eikelboom, A.W. Weeper, F.M. Schuurmans, W.C. Sinke, P.F.A. Alkemade, P.M. Sarro, C.H.M. Marea, L.A. Verhoef, *Sol. Energy Mater. Sol. Cells* **40**, 297 (1996)
57. S.K. Tripathy, *Opt. Mater.* **46**, 240 (2015)
58. C. Sosa, J. Andzelm, B.C. Elkin, E. Wimmer, K.D. Dobbs, D.A. Dixon, *J. Phys. Chem.* **96**, 6630 (1992)
59. J. Murray, K. Sen, *Molecular Electrostatic Potentials: Concepts and Applications*, 1st edn. (Elsevier, Amsterdam, 1996)
60. E. Scrocco, J. Tomasi, *Adv. Quant. Chem.* **11**, 115 (1978)

Publisher's Note Springer Nature remains neutral with regard to jurisdictional claims in published maps and institutional affiliations.